

Single crystal growth, structural and transport properties of bad metal RhSb₂*

D S Wu(吴德胜)^{1,2}, Y T Qian(钱玉婷)^{1,2}, Z Y Liu(刘子懿)^{1,2}, W Wu(吴伟)^{1,2},
Y J Li(李延杰)^{1,2}, S H Na(那世航)^{1,2}, Y T Shao(邵钰婷)^{1,2}, P Zheng(郑萍)^{1,2},
G Li(李岗)^{1,2,3}, J G Cheng(程金光)^{1,2,3}, H M Weng(翁红明)^{1,2,3}, and J L Luo(雒建林)^{1,2,3,†}

¹Beijing National Laboratory for Condensed Matter Physics, Institute of Physics, Chinese Academy of Sciences, Beijing 100190, China

²School of Physical Sciences, University of Chinese Academy of Sciences, Beijing 100190, China

³Songshan Lake Materials Laboratory, Dongguan 523808, China

(Received 9 December 2019; revised manuscript received 2 January 2020; accepted manuscript online 9 January 2020)

We have successfully grown an arsenopyrite marcasite type RhSb₂ single crystal, and systematically investigated its crystal structure, electrical transport, magnetic susceptibility, heat capacity, and thermodynamic properties. We found that the temperature-dependent resistivity exhibits a bad metal behavior with a board peak around 200 K. The magnetic susceptibility of RhSb₂ shows diamagnetism from 300 K to 2 K. The low-temperature specific heat shows a metallic behavior with a quite small electronic specific-heat coefficient. No phase transition is observed in both specific heat and magnetic susceptibility data. The Hall resistivity measurements show that the conduction carriers are dominated by electrons with $n_e = 8.62 \times 10^{18} \text{ cm}^{-3}$ at 2 K, and the electron carrier density increases rapidly above 200 K without change sign. Combining with *ab-initio* band structure calculations, we showed that the unusual peak around 200 K in resistivity is related to the distinct electronic structure of RhSb₂. In addition, a large thermopower $S(T)$ about $-140 \mu\text{V/K}$ is observed around 200 K, which might be useful for future thermoelectric applications.

Keywords: single crystal growth, *ab-initio* band calculations, susceptibility, heat capacity, thermodynamic transport properties

PACS: 81.10.-h, 71.20.-b, 52.25.Fi

DOI: 10.1088/1674-1056/ab696e

1. Introduction

Many new 4d or 5d-electron based materials have been synthesized, and their exotic physical properties have been discovered and extensively studied in recent years. Compared to the 3d-electron based ones, they are less localized and have weaker correlation effects. But they have stronger spin-orbit coupling (SOC), which makes many of them novel topological materials or thermoelectric materials, such as WTe₂, TaAs, ZrTe₅, and HfTe₅.^[1-6] These materials have attracted extensive interests in the condensed-matter physics due to their nontrivial band topology and novel physical properties such as chiral thermal and electric transport behaviors. It has also been suggested that some narrow-gap semiconductors or semimetals of 3d-electron materials will have huge thermopowers like FeSb₂ and CoSb₂.^[7-9] For example, FeSb₂ crystallized in the marcasite-type orthorhombic structure was reported to be a narrow band nearly magnetic or Kondo semiconductor. The thermopower $S(T)$ of FeSb₂ could reach as high as 40 mV/K.^[10] CoSb₂ belongs to the pyrite-marcasite fam-

ily. The thermopower $S(T)$ of CoSb₂ could reach 40 $\mu\text{V/K}$ at room temperature.^[9] We have noticed that RhSb₂ crystallizes in arsenopyrite-marcasite type structure which is isostructural to that of CoSb₂, and its powder sample was synthesized decades ago. However, its physical properties have not been well characterized so far. The room-temperature resistivity of the polycrystalline sample is 0.002 $\Omega\cdot\text{cm}$, and the thermoelectric power is reported to be +30 $\mu\text{V/K}$.^[7] The magnetic susceptibility of RhSb₂ shows Landau diamagnetism.^[7,11,12] Therefore, to find new d-electron based materials with nontrivial topological band structure or exitonic physical properties is meaningful.

Transport properties are important for the application in devices as conducting materials. Generally, the resistivity of a normal metal increases with increasing temperature T because the phonon scattering of conducting electrons gets stronger at higher temperatures. For a semiconductor, the transport properties are dominated by the number of carriers, the resistivity decreases with increasing T due to the increased thermal activated carriers at higher temperatures. However, in some ma-

*Project supported by the National Natural Science Foundation of China (Grant Nos. 11674375, 11634015, 11925408, and 11674369), the National Basic Research Program of China (Grant Nos. 2016YFA0300600, 2016YFA030240, 2017YFA0302901, and 2018YFA0305700), the Strategic Priority Research Program and Key Research Program of Frontier Sciences of the Chinese Academy of Sciences (Grant Nos. QYZDB-SSW-SLH013, XDB28000000, and XXH13506-202), the Science Challenge Project of China (Grant No. TZ2016004), the K. C. Wong Education Foundation, China (Grant No. GJTD-2018-01), the Beijing Natural Science Foundation, China (Grant No. Z180008), and the Beijing Municipal Science and Technology Commission, China (Grant No. Z181100004218001).

†Corresponding author. E-mail: jlluo@iphy.ac.cn

materials, the resistivity shows non-monotonic temperature dependences. For example, the temperature dependent resistivity of ZrTe_5 or HfTe_5 shows a broad peak around 65 K or 135 K.^[13–20] It was explained either by a temperature induced Lifshitz transition observed in angle-resolved photoemission (ARPES) experiments,^[21] or a topological band phase transition.^[22] A sign change of thermopower S_{xx} is observed which might respond to the topological band structure.^[23–25] Thus, it is of great interest to find similar transport behavior in other materials which may shed light in understanding the origin of the unusual transport behavior observed in ZrTe_5 and HfTe_5 .

In this work, for the first time we successfully grew RhSb_2 single crystals, and carried out detailed studies on its structure and basic physical properties, especially for the investigation of its unusual transport properties. We found that the temperature-dependent resistivity exhibits a bad metal behavior with a broad peak around 200 K, which is similar to the situation in ZrTe_5 . The Hall resistivity measurements show that the conduction carriers are dominated by electrons, and the electron carrier density increases rapidly above 200 K. Combined with the electron band structure calculation, our analysis shows that the usual peak and the abruptly increases in carrier density around 200 K are related to the distinct electronic structure of this material. In addition, the magnetic susceptibility shows diamagnetism in the measured temperature range from 2 K to 300 K. The low temperature specific heat shows a metallic behavior with electronic coefficient of $1.09 \text{ mJ}\cdot\text{mol}^{-1}\cdot\text{K}^{-2}$. No phase transition is observed in susceptibility and specific heat data. Furthermore, we also carried the thermopower measurements and found that the thermopower is negative and its maximum absolute value $|S_{\text{max}}|$ is about $140 \mu\text{V}/\text{K}$ at 200 K without any sign change in the whole temperature range.

2. Experiment details and calculation methodology

Single crystals of RhSb_2 were grown by self-flux method mentioned elsewhere.^[9] The starting materials, Rh (99.99%) and Sb (99.999%, Alfa), were mixed together with the mole ratio 1 : 20 in Al_2O_3 capsules which were sealed into a quartz tube. The whole quartz tube was then quickly heated up to 1273 K in a furnace and maintained at this temperature for several hours. Then it was cooled down to 1073 K where the flux was spun off by a centrifuge. Finally, crystals with approximate dimensions $2 \text{ mm}\times 2 \text{ mm}\times 1 \text{ mm}$ were left in the capsules. The crystals were stable in air and hydrochloric acid. To confirm the stoichiometry, the chemical compositions of the crystal were confirmed by energy dispersive x-ray spectroscopy (EDS) equipped on a Hitachi S-4800 scanning electron microscope (SEM). The crystals were characterized by

x-ray diffraction (XRD) at 300 K on a Bruker SMART APEX II diffractometer using $\text{Mo } K\alpha 1$ radiation ($\lambda = 0.71073 \text{ \AA}$). The crystal structure was refined by full-matrix least-squares fitting on F2 using the SHELXL-2014/7 program.^[26] A well-crystallized sample was selected for the measurements. The magnetic susceptibility χ was measured in a Quantum Design SQUID VSM from 300 K to 2 K in field-cooling (FC) and zero-field cooling (ZFC) modes. The specific heat C_p was measured between 2 K and 300 K in a physical property measurement system (PPMS, Quantum Design) using a thermal relaxation method, approximately 12 mg of crystals were used for the specific heat measurements. The ρ_{xx} and the Hall coefficient data were measured upon cooling from 300 K to 2 K using a standard four-probe technique with a gauge current of 1 mA. Platinum wires and silver paste were used to make electrical contacts on RhSb_2 single crystal. The angle dependent magnetic resistance data were collected with a lock-in technique at 2 K in the PPMS system. The first-principles calculations were performed using the Vienna *ab-initio* simulation package (VASP)^[27,28] and the generalized gradient approximation (GGA) with the Perdew–Burke–Ernzerhof (PBE)^[29] type exchange–correlation potential was adopted. We set 400 eV cutoff energy for the plane wave expansion and used $11 \times 11 \times 11$ k -mesh for the Brillouin zone (BZ) in self-consistent calculations. The crystal structure from our EDS was exploited. The electronic structures both without and with spin–orbit coupling (SOC) were obtained.

3. Results and discussion

RhSb_2 crystallizes in a pyrite-marcasite type structure in space group $P2_1/c$ (No. 14), as shown in Fig. 1(a). The crystal structure of RhSb_2 can be viewed as individual Rh along the c axis, and each Rh is surrounded by four polyhedral Sb in the ab plane. Figure 1(b) shows the single-crystal XRD data at room temperature. The large surface of the crystals characterized by XRD indicates the [011] direction of the large face. The typical size of the RhSb_2 single crystals is $2 \text{ mm}\times 2 \text{ mm}\times 0.5 \text{ mm}$, as shown by an optical image in the upper inset of Fig. 1(b). The composition was checked by EDS. The results show that the chemical ratios of the RhSb_2 crystals are 1 : 2 within the experiment accuracy of 5%. The quality of the crystals was then checked by single crystal x-ray diffraction at room temperature in a Bruker D8 Venture diffractometer using $\text{Mo } K\alpha$ radiation, $\lambda = 0.71073 \text{ \AA}$. The structure refined results indicate a stoichiometric composition with the monoclinic type structure (space group $P2_1/c$, No. 14). Structure refinement was performed by the program SHELXL-2014/7^[22] embedded in the program suite Apex3. Employing the known crystal structure of RhSb_2 , the best refinement had R -indices of $R = 0.0334(74)$ and $wR2 = 0.0767(74)$, respectively. The lattice parameters

$a = 6.6172(6)$ Å, $b = 6.5635(6)$ Å, and $c = 6.6873(6)$ Å, in accordance with the reported values.^[7]

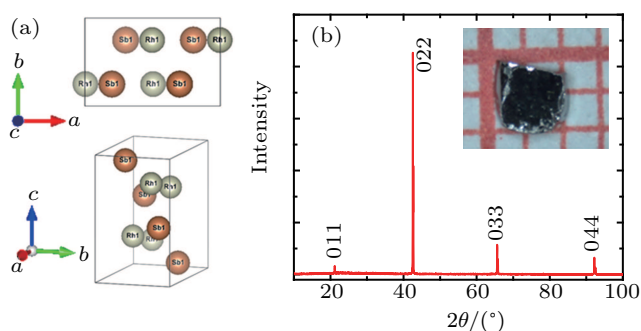


Fig. 1. (a) Crystal structure of RhSb₂ showing Rh surrounded by Sb octahedra at room temperature. (b) Single crystal XRD pattern of RhSb₂ at room temperature. The inset shows the picture of typically selected crystals.

Figure 2(a) shows the temperature-dependent resistivity $\rho(T)$ of RhSb₂ from 2 K to 300 K for samples A and B. The resistivity of sample A increases with lowering temperature to about 200 K, and then decreases upon further cooling down. A large broad peak around 200 K is clearly observed, which is similar to ZrTe₅ at zero field. The $\rho(T)$ of RhSb₂ is different from that of normal metals. While around 20 K, a small peak is observed for both sample A and sample B. The value of resistivity is between 15 mΩ·cm and 30 mΩ·cm, indicating that RhSb₂ is a bad metal.

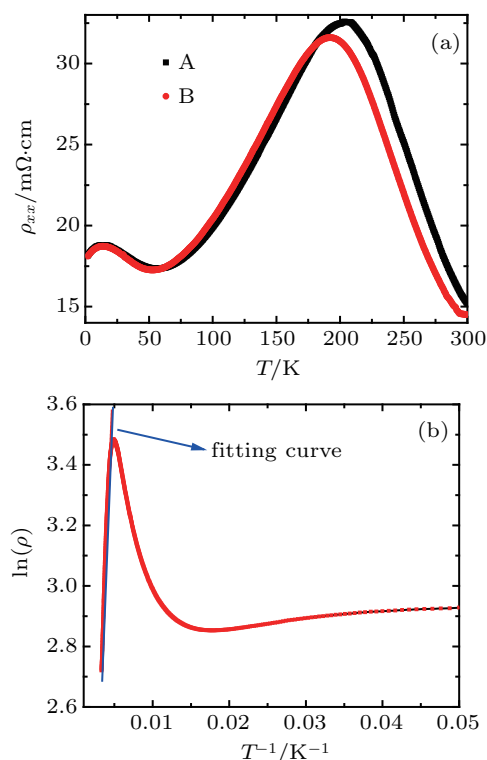


Fig. 2. (a) Temperature dependence of the longitudinal resistivity ρ_{xx} from 2 K to 300 K at zero field for different RhSb₂ samples of A and B. (b) $\ln(\rho)$ vs. $1/T$ curve of sample A. The blue line is the linear fit at temperatures above 200 K.

The large peak observed in $\rho(T)$ at 200 K might be related to exotic physical mechanisms. To confirm whether the

peak in the resistivity data is corresponding to a phase transition nor not, we carried out the magnetic susceptibility and specific heat measurements on RhSb₂ single crystals. Figure 3(a) shows the temperature-dependent magnetic susceptibility $\chi(T)$ of RhSb₂. $\chi(T)$ displays diamagnetism and is almost temperature independent above 20 K, and then increases upon further cooling below 20 K. Neither anomalies signifying magnetic orderings nor clear abruptions between the ZFC and FC curves are visible. The $\chi(T)$ is in fact very small, for example, $\chi(2$ K) is only about -0.9×10^{-4} emu·mol⁻¹·Oe⁻¹ in the magnetic field of $H = 10$ kOe. There is a small tail in the χ - T curve near 2 K, which might be contributed by a magnetic impurity effect. The diamagnetic behavior is also confirmed by the isothermal magnetization shown in Fig. 3(b) measured at 2 K and 300 K. No clear hysteresis loops are visible in the $M(H)$ curves at both temperatures of 2 K and 300 K.

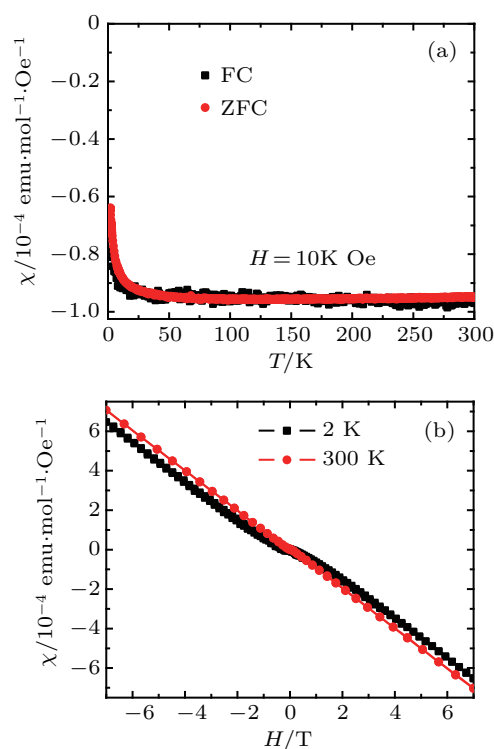


Fig. 3. (a) Temperature dependence of the dc magnetic susceptibility with ZFC and FC measured in a field of 1 T. (b) The magnetic hysteresis of the sample measured at 2 K and 300 K.

Temperature-dependent specific heat ($C_p(T)$) of RhSb₂ is presented in Fig. 4(a). The heat capacity changes rather monotonically without showing any anomalies, suggesting the absence of any structural or magnetic transitions in the measured temperature range. The heat capacity $C_p(300$ K) is approximately 74.36 J·mol⁻¹·K⁻¹, close to the value estimated from the classical Dulong–Petit heat capacity $C_p = 3nR \approx 74.94$ J·mol⁻¹·K⁻¹, where $n = 3$ is the atoms number of per formula unit and R is the molar gas constant. No Schottky-like anomalous is found in $C_p(T)$. Thus, it is reasonable to describe the specific heat of the samples as the sum of

electronic and lattice contributions at low temperatures with formula $C_p(T)/T = \beta T^2 + \gamma$, where β and γ are the lattice and electronic contributions to $C_p(T)$, respectively. The low-temperature specific heat below 10 K is shown in the form $C_p(T)/T$ vs. T^2 as an inset to Fig. 4(b). The linear trend of the plot at very low temperatures indicates that the Debye approximation may characterize the temperature dependence of $C_p(T)$. The least-squares analysis to the linear part using the above formula yields $\gamma \approx 1.09 \text{ mJ}\cdot\text{mol}^{-1}\cdot\text{K}^{-2}$. The non-zero γ value shows a considerable density of states (DOS) at E_F , indicating a metallic behavior of RhSb₂, consistent with a bad metal that observed in the low temperature resistivity.

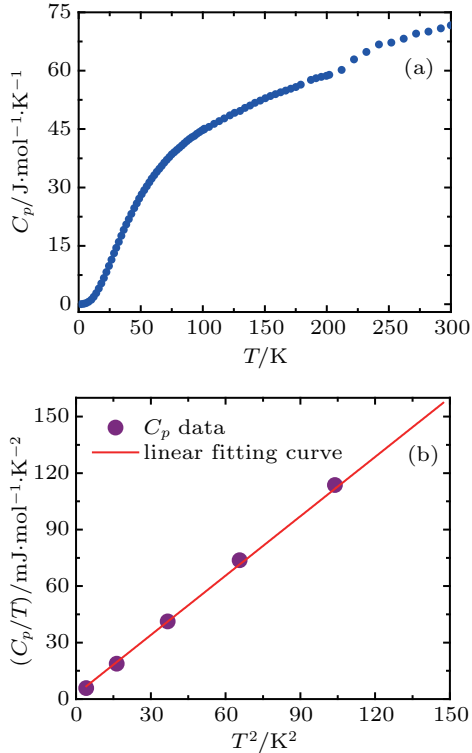


Fig. 4. (a) Specific heat C_p as a function of T . (b) C_p/T versus T^2 for a RhSb₂ sample. The red line is the linear fitting data of C_p/T versus T^2 at low temperature below 10 K.

The above susceptibility and specific heat measurements suggest that the resistivity peak at about 200 K is not due to a phase transition. We find that such behavior may be understood by the distinct electronic structure in RhSb₂. The band structure calculated within GGA is shown in Fig. 5 with and without considering SOC. When considering SOC, there is a tiny electron pocket cross the Fermi level at E point, while there is a very small gap at another high symmetry point Y_2 . At low temperatures, the tiny electron pocket contributes a small amount of electron carriers, thus $\rho(T)$ shows the metallic behavior. Since the gap at Y_2 point is considerably small of 0.074 eV, with raising temperature, some carriers could be thermally activated above the Fermi level and then the resistivity decreases with further raising temperature due to the additional thermally activated charge carriers. The thermally acti-

vated term in resistivity can be expressed by $\rho = Ce^{-\Delta/k_B T}$.^[30] Figure 2(b) shows the fitting of the resistivity data of sample A using this formula. From the fitting, we can obtain the energy gap Δ at Y_2 point to be 0.052 eV, which is comparable with the theoretical value of 0.074 eV.

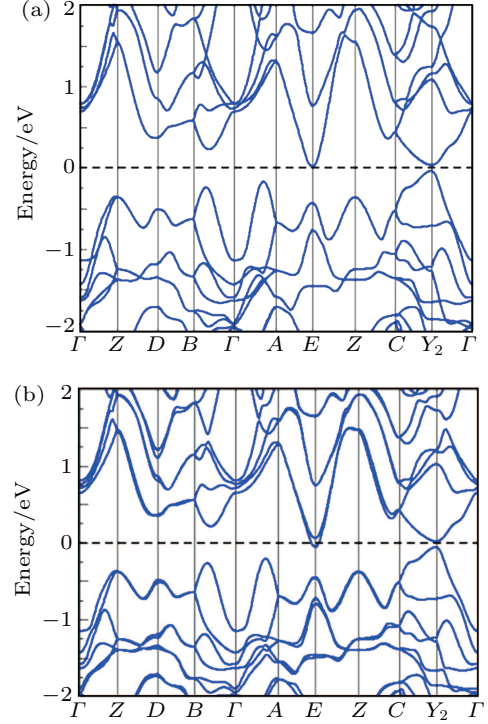


Fig. 5. The electronic structures of RhSb₂: (a) without SOC and (b) with SOC.

In order to check whether the temperature induced Lifshitz transition happened around 200 K in RhSb₂, just like the situation in ZrTe₅,^[20,21] figure 6(a) presents the field dependence resistivity ρ_{xx} and ρ_{xy} of RhSb₂ at 2 K. The applied magnetic field is along [011] direction, perpendicular to the direction of the electric current. Both the Hall signal mixed into ρ_{xx} can be removed by averaging the raw data ρ_{xx} over the positive and the negative field directions. From the raw ρ_{xx} data measured at different temperatures, we obtained the symmetrized (intrinsic) longitudinal resistance, which is plotted as MR = $[\rho_{xx}(H)/\rho_{xx}(0 \text{ T}) - 1] \times 100\%$ in Fig. 6(b). MR of RhSb₂ is just several percentages and changes slightly with temperature, which is different from that in the previous reported topological materials like Dirac semimetal Cd₃As₂,^[31–34] type II Weyl semimetal WTe₂, etc.^[1] As shown in Fig. 6(c), below 200 K, the linear field dependence and the negative slope in Hall resistivity confirm that the electron carriers dominate the transport behavior. The temperature-dependent Hall resistivity measurements show no sign change. Using a single band model, the carrier density at 2 K can be deduced from the Hall coefficient using $R_H = -1/n_e$ to be $n_e = 8.62 \times 10^{18} \text{ cm}^{-3}$. Indeed, the magnitude of n_e is 4–5 orders smaller than that of a normal metal, consistent with the existence of a tiny elec-

tron pocket at Fermi energy at E point in the band calculations. Above 200 K, the Hall resistivity remains linear field-dependent with negative slope, indicating that electron carriers still dominate the transport properties. The temperature dependence of n_e is plotted in Fig. 6(d). It can be seen that n_e is almost constant below ~ 200 K, whereas n_e increases to $n_e = 1.31 \times 10^{20} \text{ cm}^{-3}$, about 15 times larger than the value at 2 K. This indicates that a large number of thermally activated carriers are induced above 200 K, which is consistent with the existence of very small gap at Fermi energy at Y_2 point.

Besides, we also studied the thermoelectric transport properties of RhSb₂. As shown in Fig. 7, the thermopower $S(T)$ of RhSb₂ is negative in the whole temperature range be-

low room temperature, consistent with the band-structure calculation and Hall resistivity measurements. The $S(T)$ follows the same trend as the resistivity, i.e., $|S(T)|$ increases with temperature, attends a maximum value of $\sim 140 \mu\text{V/K}$ at 200 K, and then decreases gradually to $\sim 70 \mu\text{V/K}$ at 300 K, which is much larger than the previously reported value of $30 \mu\text{V/K}$ in a polycrystalline sample at room temperature. However, the maximum value of $|S(T)| \sim 140 \mu\text{V/K}$ is much smaller than the reported value of 40 mV/K for FeSb₂.^[7,10] No sign change of $S(T)$ in RhSb₂ was observed, indicating that the electron carriers dominate the transport properties in the investigated temperature range.

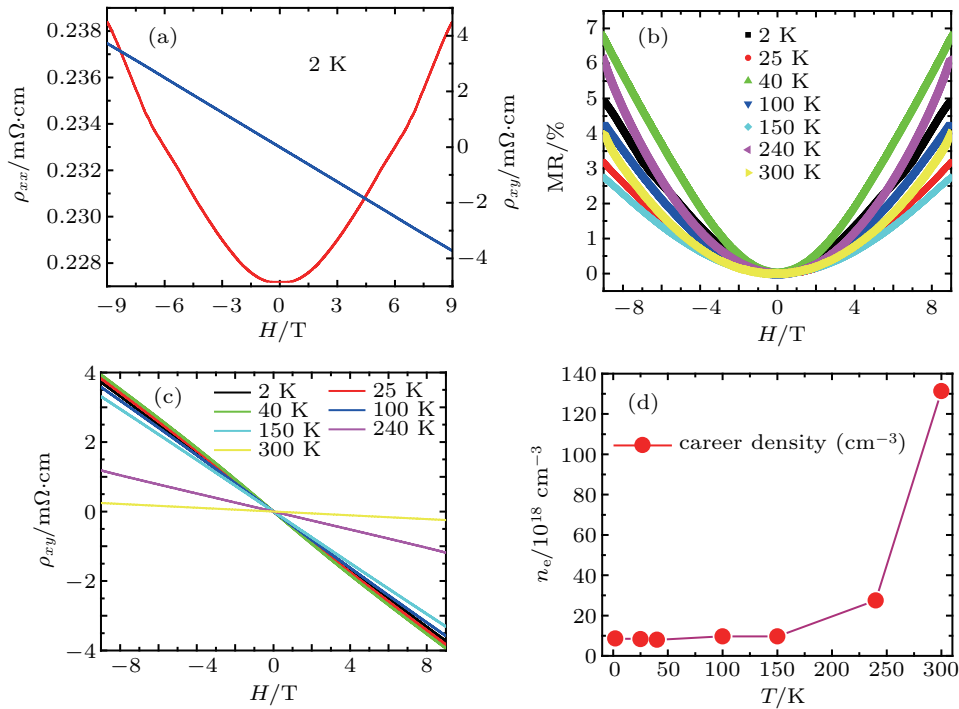


Fig. 6. (a) ρ_{xx} and ρ_{xy} of RhSb₂ single crystal at 2 K with applying magnetic field along [011] direction, (b) MR measured at different temperatures with fields along the [011] axis. (c) The Hall resistivity vs. magnetic field B at different temperatures of 2 K, 25 K, 40 K, 100 K, 150 K, 240 K, 300 K. (d) The concentration of carriers is obtained by fitting the Hall conductivity with a single-band model.

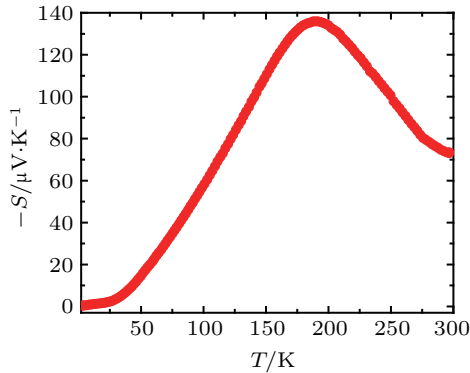


Fig. 7. Temperature dependence of the thermopower $S(T)$ of RhSb₂ single crystals from 2 K to 300 K.

Similar $\rho(T)$ with a peak at a certain temperature has also been observed in ZrTe₅ and HfTe₅ and the underline mechanism has been a puzzle for a long time.^[14,17,18] Recently,

it was proposed that a topological phase transition between strong and weak topological insulators might be the reason for it.^[3] However, in ZrTe₅ and HfTe₅, the diamagnetism is strongly temperature dependent and $S(T)$ changes sign around the peak of $\rho(T)$.^[16,25] These mean that RhSb₂ is more like a narrow band gap semiconductor with a tiny electron pocket as shown in the GGA band structure. The small band gap around Y_2 is tunable by strain or pressure effect. It is found that the critical uniaxial strain along c -axis and the hydrostatic pressure are both about 5% to drive the topological phase transition from a normal insulator to a strong topological insulator. Magnetic ion-doping can introduce spin dependent exchange interaction, which will compete with such small band gap and lead to topological states, such as magnetic Weyl semimetal and axion insulator.

4. Conclusion

We have successfully grown RhSb₂ single crystal by Sb flux method. We present the structure, electron transport, heat capacity, magnetic, thermal transport properties of the bad metal d-electron compound RhSb₂. The RhSb₂ compound crystallizes into an arsenopyrite structure in space group $P2_1/c$. The temperature-dependent resistivity exhibits a bad metal behavior with a broad peak around 200 K. The Hall resistivity measurements show that the dominant conduction carriers are electrons, and the electron carrier density increases rapidly above 200 K without any sign change. Together with the band calculations, we found that the unusual peak and abruptly increases in carrier density around 200 K are related to the topological electronic band structure of this material. In addition, the magnetic susceptibility shows diamagnetism in the measured temperature range from 2 K to 300 K. No phase transition is observed in susceptibility and specific heat data, which supports our calculations. Furthermore, we also carried the thermopower measurements and found that the thermopower is negative and its maximum absolute value $|S_{\max}|$ is about 140 $\mu\text{V}/\text{K}$ at 200 K, which will be helpful for future device applications.

Acknowledgments

We thank Dr. J. H. Zhang, J. P. Sun, Prof. G. T. Liu, Prof. Z. G. Chen for fruitful discussion. The authors are grateful to Dr. Y. T. Song (Institute of Physics) for his help in x-ray experiments.

References

- [1] Ali M N, Xiong J, Flynn S, Tao J, Gibson Q D, Schoop L M, Liang T, Haldolaarachchige N, Hirschberger M, Ong N P and Cava R J 2014 *Nature* **514** 205
- [2] Weng H M, Fang C, Fang Z B, Bernevig A and Dai X 2015 *Phys. Rev. X* **5** 011029
- [3] Weng H M, Fang Z and Dai X 2014 *Phys. Rev. X* **4** 011002
- [4] Lv B Q, Weng H M, Fu B B, Wang X P, Miao H, Ma J and Fang Z 2015 *Phys. Rev. X* **5** 031013
- [5] Wieting T J, Gubser D U, Wolf S A and Levy F 1980 *Bull. Am. Phys. Soc.* **25** 340
- [6] Okada S, Sambongi T and Ido M 1980 *J. Phys. Soc. Jpn.* **49** 839
- [7] Johnston W D, Miller R C and Damon D H 1965 *J. Less-Common Met.* **8** 272
- [8] Hulliger F 1964 *Nature* **201** 4917
- [9] Kjekshus A 1971 *Acta Chem. Scand.* **25** 441
- [10] Sun P, Oeschler N, Johnsen S, Iversen B B and Steglich F 2009 *Phys. Rev. B* **79** 153308
- [11] Takahashi H, Okazaki R, Yasui Y and Terasaki I 2011 *Phys. Rev. B* **84** 205215
- [12] Hulliger F 1963 *Phys. Lett.* **4** 282
- [13] Furuseth S, Brattas L and Kjekshus A 1973 *Acta Chem. Scand.* **27** 2367
- [14] DiSalvo F J, Fleming R M and Waszczak J V 1981 *Phys. Rev. B* **24** 2935
- [15] Liu Y, Yuan X, Zhang C, Jin Z, Narayan A, Luo C and Sanvito S 2016 *Nat. Commun.* **7** 12516
- [16] Jones T E, Fuller W W, Wieting T J and Levy F 1982 *Solid State Commun.* **42** 793
- [17] Izumi M, Uchinokura K, Matsuura E and Harada S 1982 *Solid State Commun.* **42** 773
- [18] McLroy D N, Moore S, Zhang D, Wharton J, Kempton B, Littleton R and Olson C G 2004 *J. Phys.: Condens. Matter* **16** 30
- [19] Liang T, Lin J, Gibson Q, Kushwaha S, Liu M, Wang W and Shen Z X 2018 *Nat. Phys.* **14** 451
- [20] Chen R Y, Zhang S J, Zhang A Q, Gu G D and Wang N L 2015 *Phys. Rev. B* **92** 075107
- [21] Zhang Y, Wang C, Yu L, Liu G, Liang A, Huang J, Dong L G and Zhou X J 2017 *Nat. Commun.* **8** 15512
- [22] Manzoni G, Gragnaniello L, Autès G, Kuhn T, Sterzi A, Cilento F and Bisti F 2016 *Phys. Rev. Lett.* **117** 237601
- [23] Smontara A, Biljakovi K, Miljak M and Sambong T 1986 *Physica B* **143** 267
- [24] Hooda M K and Yada C S 2017 *Appl. Phys. Lett.* **111** 053902
- [25] Zhang J L, Wang C M, Guo C Y, Zhu X Zhang D, Yang Y and Tian M L 2019 *Phys. Rev. Lett.* **123** 196602
- [26] <http://shelx.uni-goettingen.de>
- [27] Kresse G and Furthmüller J 1996 *Phys. Rev. B* **54** 11169
- [28] Kresse G and Joubert D 1999 *Phys. Rev. B* **59** 17953
- [29] Blöchl P E 1994 *Phys. Rev. B* **50** 17953
- [30] Fang Y, Ran S, Xie W, Wang S, Meng Y S and Maple M B 2018 *Proc. Natl. Acad. Sci. USA* **115** 8558
- [31] He L P, Hong X C, Dong J K, Pan J, Zhang Z, Zhang J and Li S Y 2014 *Phys. Rev. Lett.* **113** 246402
- [32] Neupane M, Xu S Y, Sankar R, Alidoust N, Bian G and Liu B A 2014 *Nat. Commun.* **5** 3786
- [33] Zhao Y, Zhang H, Liu C, Wang H, Wang J, Lin Z and Brombosz S M 2015 *Phys. Rev. X* **5** 031037
- [34] Feng J, Pang Y, Wu D, Wang Z, Weng H, Li J and Lu L 2015 *Phys. Rev. B* **92** 081306(R)
- [35] Martino E, Crassee I, Eguchi G, Santos C D, Zhong R D, Gu G D and Akrap A 2019 *Phys. Rev. Lett.* **122** 217402